Autonomous metabolic reprogramming and oxidative stress characterize endothelial dysfunction in acute myocardial infarction

Erika Zodda[1,2,3], Olga Tura-Ceide[4,5,6], Nicholas L. Mills[7], Josep Tarragó-Celada[1], Marina Carini[8], Timothy M Thomson[2,3,9#*], Marta Cascante[1,3,10#*]

1 Department of Biochemistry and Molecular Biology, Faculty of Biology, University of Barcelona, Spain

2 Institute for Molecular Biology of Barcelona, National Research Council (IBMB-CSIC), Barcelona, Spain

3 Centro de Investigación Biomédica en Red de Enfermedades Hepáticas y Digestivas (CIBER-EDH), Madrid, Spain

4 Department of Pulmonary Medicine, Hospital Clínic-Institut d'Investigacions Biomèdiques August Pi I Sunyer (IDIBAPS); University of Barcelona; Barcelona, Spain

5 Centro de Investigación Biomédica en Red de Enfermedades Respiratorias (CIBER-ER), Madrid, Spain

6 Department of Pulmonary Medicine, Dr. Josep Trueta University Hospital de Girona, Santa Caterina Hospital de Salt and Girona Biomedical Research Institute (IDIBGI), Girona, Spain

7 University/BHF Centre for Cardiovascular Science, University of Edinburgh, United Kingdom

8 Department of Pharmaceutical Sciences, Università degli Studi di Milano, Milan, Italy

9 Universidad Peruana Cayetano Heredia, Lima, Peru

10 Institute of Biomedicine (IBUB), University of Barcelona, Barcelona, Spain

#These authors contributed equally to this work

*Corresponding authors

Correspondence: Marta Cascante, Department of Biochemistry and Molecular Biomedicine, Faculty of Biology, Universitat de Barcelona. Institute of Biomedicine of Universitat de Barcelona (IBUB) and CSIC-Associated Unit. Av Diagonal 643, Barcelona 08028, Spain. Tel: +34-93-402-1217. Fax: +34-93-402-1559. Email: martacascante@ub.edu; Timothy M. Thomson, Barcelona Institute for Molecular Biology (IBMB-CSIC), c. Baldiri Reixac 15-21, 08028 Barcelona, Spain; e-mail titmc@ibmb.csic.es.

Abstract

Background: Compelling evidence has accumulated on the role of oxidative stress on the endothelial cell (EC) dysfunction underlying acute coronary syndrome. However, unveiling the underlying metabolic determinants has been hampered by the scarcity of appropriate cell models to address cell-autonomous mechanisms of ED dysfunction.

Methods: We have generated endothelial cells derived from thrombectomy specimens from patients affected with acute myocardial infarction (AMI) and conducted phenotypical and metabolic characterization, focused on central carbon metabolism.

Results: AMI-derived endothelial cells (AMIECs), but not control healthy coronary endothelial cells, display impaired growth, migration and tubulogenesis. Metabolically, AMIECs displayed augmented reactive oxygen species (ROS) and glutathione intracellular content, along with a diminished glucose consumption coupled to high lactate production. Consistent with diminished glycolysis in AMIECs, the protein levels of 6-phosphofructo-2-kinase/fructose-2,6-bisphosphatase type 3, PFKFB3, were downregulated. In contrast, PFKFB4 levels were upregulated, suggesting a shunting of glycolysis towards the pentose phosphate pathway (PPP), supported by upregulation in AMIECs of G6PD, the key enzyme in the oxidative branch of the PPP. Further, the glutaminolytic enzyme GLS was upregulated in AMIECs, providing a mechanistic explanation for the observed increase in glutathione content. Finally, AMIECs displayed a significantly higher mitochondrial membrane potential than control ECs, which, together with high ROS levels, suggest a highly coupled mitochondrial activity in patient ECs.

Conclusions: We suggest high mitochondrial proton coupling underlies the abnormally high production of ROS, balanced by PPP- and glutaminolysis-driven synthesis of glutathione, as a primary, cell-autonomous abnormality driving EC dysfunction in AMI.

Funding: European Commission Horizon 2020; CIBER- Carlos III National Institute of Health, Spain; Ministerio de Economia y Competitividad (MINECO) and Ministerio de Ciencia e Innovación, Spain; Generalitat de Catalunya-AGAUR, Catalonia;

Plataforma Temática Interdisciplinar Salud Global (PTI-SG), Spain; British Heart Foundation, UK.

Introduction

Cardiovascular diseases are the leading cause of death worldwide and comprise a range of syndromes affecting the functionality of the heart and blood vessels (*Smolders et al., 2018; Townsend et al., 2022*). Vascular dysfunction is believed to be a primary factor in the onset and progression of atherosclerosis and other vascular-related disorders. In this study, we focus our attention on a specific vascular disease, acute myocardial infarction (AMI), a major cause of morbidity in the Western world (Townsend et al., 2022). AMI occurs as a consequence of coronary occlusion, generally from a thrombus superimposed on an ulcerated or unstable atherosclerotic plaque (*Badimon et al., 2012; Smolders et al., 2018*). The endothelium plays a pivotal role in the development of AMI, both preceding atherogenesis and predisposing to thrombosis (*Previtali et al., 2011*).

Emerging evidence indicates that pathological blood vessel responses and endothelial dysfunction are associated with metabolic alterations in ECs (*Botts et al., 2021; Moreno-Viedma et al., 2016*). Thus, to identify new strategies to limit CVD progression in at risk/affected patients, metabolic alterations underlying impaired endothelial cells functions require appropriate patient-derived cell models (*Gallogly et al., 2021*). As such, the study of endothelial metabolism and mitochondrial function may be central to unveiling fundamental mechanisms of cardiovascular pathogenesis, and to identify novel critical metabolic biomarkers and therapeutic targets.

Here, we have approached the study of endothelial cells dysfunction and metabolic alterations associated with AMI, by using coronary endothelial cells isolated and cultured from thrombectomy specimens obtained from patients affected with AMI. Our observations point to pharmacologically actionable cell-autonomous metabolic dysfunction in these cells.

Results

AMIECs display impaired growth and migration

AMIECs were isolated from coronary atherothrombotic specimens from 8 patients undergoing percutaneous coronary intervention with thrombectomy for the treatment of acute ST-segment elevation myocardial infarction (STEMI). Hereafter, the 8

patient-derived cell lines are designated CE followed by two digits (CE45, CE46, CE48, CE51, CE52, CE53, CE60, CE61).

At 80% confluence, AMIECs presented the expected shape and appeared similar to control HCAECs (Fig. 1A), as expected for bona-fide endothelial cells grown under equivalent conditions. The endothelial nature of these cells was confirmed by Western blotting for the expression of the endothelial markers, V-CAM1 (vascular cell adhesion protein 1, CD-106), PECAM-1 (platelet endothelial cell adhesion molecule, CD31), CD-34 and CD-105 (endoglin) (Fig. 1B, C).

Because optimal growth conditions for endothelial cells entails maintaining them at a relatively high confluence, they cannot be kept in culture for prolonged periods at an optimal confluence (70-80%), as overgrowth will cause cells to pile up and lose their physiological monolayer growth pattern. Therefore, cell growth monitoring was limited to 168 hours. Under these conditions, all AMIECs consistently displayed slower growth rates as compared to control HCAECs (Fig. 1D). Indeed, after 168 hours, while control HCAECs had reached a plateau in their growth, AMIECs continued to proliferate exponentially, albeit at slow rates, without reaching saturation.

Given these results, we determine the cell cycle distribution of these cells by flow cytometry 24 h after seeding, the point of maximum growth in the control HCAECs. Somewhat contrary to our expectations, we observed no significant differences in the distribution of cell cycle phases between AMIECs and control cells (Fig. 1E), except for a modest tendency, without reaching statistical significance, of AMIECs to accumulate in the G1 phase relative to HCAECs. The slow growth rate, in conjunction with unaltered cell cycle phase distribution, of AMIECs suggests an overall slowing down of growth that affects equally all phases of the cell cycle.

In wound-healing migration assays, control HCAECs achieved a complete closure of the wound after 24 h of seeding (Fig. 1F). In contrast, three AMIECs displayed wound closure rates below 50%, four others about 60%, and only one about 80% after 24 h of migration under the same conditions (Fig. 1G).

These results indicate that AMI patient-derived coronary endothelial cells are dysfunctional in major cell-autonomous processes, namely growth and migration.

Defective tubulogenesis in AMIECs

The ability to migrate is a critical function of healthy endothelial cells, which can migrate while branching from existing blood vessels towards sources of angiogenic stimuli, guided by tip cells. Impairment in this fundamental endothelial function is considered a hallmark of vascular diseases (*De Bock et al., 2013*). Thus, we next assessed the tubulogenic potential of AMIECs, as an indicator of their vasculogenic (angiogenic) potential. Control HCAECs and AMIECs were cultured under conditions that favor tubulogenesis, and branching points scored after 12 h of switching to tubulogenic medium containing VEGF (Fig. 2A). While control HCAECs averaged 80 branching points, AMIECs displayed a significantly reduced tubulogenic potential, evident both as a diminished number of branching points and as shorter and fragmented tubes as compared to control cells (Fig. 2B). The branching capacity of the AMIECs derived from different patients was linearly correlated (R^2 = 0.67) with their ability to migrate (Fig. 2C) regardless of their growth rates suggesting that the deficient tubulogenesis or sprouting of these cells is linked to a defect in their migration properties, rather than to abnormal proliferation or survival.

AMIECs display low glucose consumption and high lactate production

The above characterization points to cell-autonomous defects in AMI patient-derived endothelial cells that compromise their ability to proliferate, migrate and form branched tubular structures. We next tackled the hypothesis that metabolic features of these cells might be associated with at least part of the observed phenotypes. To assess nutrient and metabolite consumption and production rates, the concentration of selected metabolites in culture media was determined. We focused on glucose as the major carbon source of the glycolytic pathway, lactate as the main metabolic end-product of glycolysis, and glutamine/glutamate as alternative sources of carbon metabolism and major providers of mitochondrial anaplerosis. We found that 6 out of the 8 AMIECs consumed glucose at significantly lower rates than control HCAECs (Fig. 3A), which may reconcile with the lower growth rates of patient-derived cells, while 2 patient-derived cell lines consumed more glucose than control cells. Remarkably, all AMIECs displayed a strong production of lactate, comparable or superior to control cells, regardless of their levels of glucose uptake (Fig. 3B).

Two of the AMIECs, CE-45 and CE-61, consumed high levels of glucose and displayed robust lactate production (Fig. 3A, B), and thus, it may be assumed that lactate is produced through glycolysis. The cells may also be hypothesized to be under a Warburg effect. However, their slow rates of proliferation stand in contrast to the rapid proliferation phenotypes seen in other cell types displaying a Warburg effect, such as cancer cells. On the other hand, the remaining 6 patient-derived endothelial cell lines, also slow growers, showed high levels of lactate production in spite of low glucose consumption (Fig. 3A, B). This uncoupling of lactate production from glycolysis suggests the existence of an alternative source of lactate in these cells. In this regard, it is worth noting that glutaminolysis also produces lactate, in a pathway that involves oxidation of glutamine to malate and then to pyruvate by the malic enzyme (ME), followed by conversion to lactate by the action of LDH-A (*Brooks, 2018*).

AMIECs shunt glycolysis towards PPP and NADPH generation

The low glucose uptake observed in 6 out of the 8 patient-derived endothelial cell lines prompted us to explore the expression of key enzymes in the glycolytic pathway. Under normal conditions, endothelial cells rely mainly on glycolysis to generate the energy required for their functions (*De Bock et al., 2013; Dromparis and Michelakis, 2013; Goveia et al., 2014*). A key rate-limiting enzyme in this pathway is phosphofructokinase 1 (PFK1), responsible for the phosphorylation of fructose-6-phosphate (F-6-P) to fructose-1,6-phosphate (F-1,6-P) in an ATP-dependent reaction. PFK1 is allosterically activated by fructose-2,6-bisphosphate (F-2,6-BP), produced from F-6-P through the catalytic activity of 6-phosphofructo-2-kinase/fructose-2,6-bisphosphatases (encoded in mammals by paralogs PFKFB1, PFKFB2, PFKFB3, PFKFB4 and TP53-induced glycolysis and apoptosis regulator (TIGAR) (*Bensaad et al., 2006; Eelen et al., 2018*). These are bifunctional enzymes bearing, on the same polypeptide, an N-terminal 6-phosphofructo-2-kinase domain, and a C-terminal fructose 2,6-bisphosphatase domain. Given its relative kinase and bisphosphatase activities, PFKFB3 is a preferred target to inhibit glycolysis over other isoforms in this family of enzymes. PFKFB3 has been described to play a significant role in the glycolytic activity of pathological ECs, and its inhibition dramatically abrogates their proliferation and migration (*Li et al., 2019; Schoors et al., 2014*).

We determined PFKFB3 protein levels by Western blotting, finding significantly lower levels in 7 out of the 8 AMIECs, as compared to control HCAECs (Fig. 4A, B), consistent with their lower glucose uptake. In fact, one of the two patient-derived cell lines with high glucose uptake, CE-45, expressed PFKFB3 at levels close to those of control cells (Fig. 4A, B), thus reinforcing the notion that cell lines with low glucose uptake have low rates of glycolysis. This may also help explain, at least in part, the low proliferation rates, migration capacity and tubulogenic activity of these cells, as these processes require robust glycolysis.

We also determined PFKFB4 protein levels, finding significantly higher levels of expression in AMIECs compared to control cells (Fig. 4A, B). Low levels of PFKFB3 expression coupled to high levels of PFKFB4 expression in AMI patient-derived cells predict a redirection of glucose-6-phosphate (G6P) towards the PPP (Yamamoto et al., 2014). As a consequence, we would expect (1) increased production of NADPH reducing equivalents through the oxidative branch of the PPP (*Dasgupta et al., 2018; Ros et al., 2017*) and (2) increased production of ribose-5-phosphate through the non-oxidative branch, for de novo synthesis of nucleotides as well as acetyl-CoA carboxylase 1 activation and lipogenesis (by inhibiting activation of liver kinase B1/AMPK signaling). The NADPH reducing equivalents produced through the non-oxidative branch afford the maintenance of redox homeostasis by scavenging reactive oxygen species (ROS) (*Benito et al., 2017; Li et al., 2014; Sun et al., 2017; Xia et al., 2017*). The nucleotides supplied through the non-oxidative branch of the PPP can be used for DNA synthesis in proliferating cells, and also in DNA damage repair (*Bester et al., 2011*).

In light of these predictions, we determined the expression level and activity of glucose-6-phosphate dehydrogenase (G6PD), the rate-limiting enzyme of the oxidative branch of the PPP. Consistently, we found significantly higher levels of G6PD in AMIECs than control cells (Fig. 4C, D). Likewise, AMIECs displayed higher levels of G6PD enzyme activity than control cells (Fig. 4E). These results support an enhanced activity of the oxidative branch of the PPP. This is expected to generate higher levels of NADPH, which, in turn, should contribute to improving ROS scavenging by maintaining glutathione in its reduced state. We thus determined ROS and glutathione levels in our cell model. Seven out of the 8 AMIECs contained ROS at significantly higher levels than control cells (Fig. 4F). The one cell line with near-

normal ROS levels, CE-45, was the same one displaying normal levels of G6PD protein (Fig. 4C, D). Similarly, the intracellular concentration of reduced glutathione was increased in all 8 AMIECs (Fig. 4G). These observations suggest that glutathione levels are upregulated in AMIECs to counter excess ROS levels.

In vivo, endothelial cells in AMI patients are under numerous physiological and pathological stresses, including mechanical and inflammatory, which may generate excess ROS and oxidative stress (*Dasgupta et al., 2018; Seo and Lee, 2014*). However, our patient-derived cells are no longer in an in vivo environment and are rather in an in vitro environment identical to that of control endothelial cells, and therefore their increased ROS levels cannot be directly attributed to environmental factors. Absent maintenance of long-term epigenetic memory of past stress responses in vivo, it is reasonable to assume that the high levels of ROS in AIM patient-derived cells may be elicited by endogenous damage signals impinging upon mitochondria (*Murphy, 2009*) or through NAD(P)H oxidases.

AMIECs exhibit a strong glutamine metabolism

Given the likely relevance of glutathione in the observed phenotypes and the possibility of a glutamine origin of the excess lactate produced in AMIECs, we assessed glutamate and cysteine contents in these cells. Determination of the extracellular fluxes of glutamine showed that the consumption of glutamine in AMIECs is higher than in control HCAECs (Fig. 5A). The latter consumed more glucose than patient-derived cells (see above), and thus the glutamine-to-glucose consumption ratio is far greater in patient-derived cells than in control cells (Fig. 5B). This suggests that AMI patient-derived cells mainly resort to glutamine, rather than glucose, as their carbon source.

Glutamine is the most abundant free amino acid in circulation and in intracellular pools, and it is used by cells for both bioenergetics and biosynthetic needs; it can act as a carbon source or nitrogen donor and is consequently used as a precursor for the synthesis of amino acids, proteins, nucleotides and lipids, and represents the main substrate for TCA cycle anaplerosis (*DeBerardinis and Cheng, 2010; Draoui et al., 2017; Fitzgerald et al., 2018; Laplante and Sabatini, 2012*). Moreover, glutamine participates in redox homeostasis, a process that has a close connection with the PPP, as one of its main functions is to generate glutathione to counter the oxidative

stress generated by ROS (see above). Thus, the increased glutamine consumption observed in AMIECs is consistent with the increased glutathione levels observed in these cells (Fig. 4G).

The anaplerotic role of glutamine requires its conversion to glutamate, in a reaction catalyzed by glutaminase (GLS). There are three isoforms of human GLS: the kidney-type (KGA) and its splice variant glutaminase C (GAC) encoded by the GLS1 gene, and the liver-type (LGA) encoded by the GLS2 gene (*Thangavelu et al., 2014; van den Heuvel et al., 2012*). Notably, the GAC isoform is crucial for cell growth under acidic pH, as would be expected in the presence of high levels of lactate (*Aguilar et al., 2016*). Given the high levels of glutamine consumption observed in patient-derived cells, we determined the expression of glutaminase by Western blotting, using isoform-specific antibodies (Fig. 5B). Consistently, both isoforms of GLS1, KGA, and GAC, are expressed at significantly higher levels in patient-derived cells than control cells (Fig. 5B, C), with a higher KGA/GAC ratio in AMIECs (Fig. 5D).

Next, polar intracellular metabolites (TCA cycle intermediates and amino acids) were determined by GC/MS. The results disclosed a higher intracellular content of all amino acids determined, with the exception of glycine, alanine, histidine and proline. Among AMIECs, CE45 displayed the intracellular amino acid profile most resembling that of control HCAECs (Fig. 5E), consistent with the overall normal-like phenotype of this cell line. Cysteine and glutamate play important roles in the synthesis of glutathione (GSH) (*Ishimoto et al., 2011*) and both had significantly higher concentrations in all AMIECs (Fig. 5E), consistent with higher levels of GSH as compared to control cells. Most of the glutamine transported into the cell is converted to glutamate by glutaminase, which is then converted to α-ketoglutarate (αKG) by glutamate dehydrogenase (GLDH). αKG is used as a carbon source for the anaplerotic replenishment of the TCA cycle, while glutamate, which normally accumulates in the cells, is a precursor of GSH. Thus, glutamate also contributes to redox homeostasis and ROS detoxification, along with the PPP. We thus determined glutamate levels in culture media, finding lower levels of production in 6 out of the 8 patient-derived cells as compared to control cells (Fig. 5F). Moreover, the ratio between glutamate production and glutamine consumption was considerably lower in AMIECs (Fig. 5G). Because of the high levels of glutaminase in patient-derived cells,

implying a strong conversion of glutamine to glutamate, the lower levels of extracellular export of glutamate are suggestive of a robust consumption of glutamate in the production of GSH in these cells.

Collectively, our data suggest that AMIECs rely heavily on glutamine, both as an alternative to glucose as a carbon source and in order to maintain redox homeostasis in these cells. Related to our observations, a link between glutamine metabolism and clinical manifestations of atherosclerosis, such as intima-media thickness and plaques development, has been described (*Grajeda-Iglesias and Aviram, 2018; Wurtz et al., 2012*).

These observations are consistent with higher levels of mitochondrial respiration and higher anaplerotic use of glutamate. The transport of glutamate into mitochondria is also essential for the biosynthesis of aspartate (*Wong et al., 2016*). Consistently, aspartate was found at increased levels in AMIECs (Fig. 5E). Aspartate derived from oxaloacetate, via glutaminolysis, produces NAD+, required for glycolysis and NADPH, needed for redox balance. Aspartate derived from oxaloacetate, via glutaminolysis, produces NAD+, required for glycolysis and NADPH, needed for redox balance (*Wong et al., 2016*). Therefore, this pathway also contributes to offset the high levels of ROS in these cells.

A possible source of the high levels of ROS observed in patient-derived cells is increased mitochondrial respiration in these cells. On the other hand, high levels of glutaminase and glutamine consumption suggest a strong activation of glutaminolysis in patient-derived cells. Once in the internal space of the mitochondria, glutamate is converted into α-ketoglutarate and ammonia by glutamate dehydrogenase, along with the reduction of $NAD(P)^+$ into NADPH. NADH is the substrate of complex I of the mitochondrial respiratory chain, and its oxidation results in the translocation of H^+ across the membrane, thus producing a proton gradient. Together, our evidence predicts an increased mitochondrial membrane potential in these cells. High membrane potential implies large negative potentials in the mitochondrial matrix, leading to glutamate expulsion and high glutaminase activity. Maintenance of the mitochondrial membrane potential (Δψm) is an essential component in the process of energy storage during oxidative phosphorylation, as it reflects the pumping of H^+ across the inner membrane during the process of electron transport and oxidative phosphorylation (*Zorova et al., 2018*).

We thus determined the status of the mitochondrial membrane potential in our cells. For this, we used the fluorescent probe DiIC1(5) (MitoProbe), a positively charged, cell-permeant dye that accumulates within the negatively-charged mitochondrial matrix. MitoProbe accumulated at significantly higher levels in all AMIECs relative to control HCAECs (Fig. 5H), indicating a mitochondrial hyperpolarization due to increased membrane potentials. The subsequent addition of the uncoupling agent carbonyl cyanide m-chlorophenylhydrazone (CCCP) resulted in rapid depolarization, reflecting the proton gradient dissipation.

Discussion

Understanding metabolic reprogramming as a paramount process driving the endothelial dysfunction that underlies atherogenic cardiovascular diseases is critical for designing new therapeutic approaches, in conjunction with conventional interventions, to tackle still unmet needs for better clinical management of these broad categories of disease. Much of the accrued evidence for metabolic and mitochondrial dysfunction in ECs in atherogenesis comes from animal models (*Negre-Salvayre et al., 2020*) or studies in patients (*Shemiakova et al., 2020*), critical scenarios to achieve contextual understanding of the pathophysiological processes at stake.

In this study, we have departed from those approaches, in an attempt to better delineate cell-autonomous metabolic features of ECs derived from AMI patients, or AMIECs. We have found that, contrary to physiologically normal ECs, which rely mostly on glycolysis for energy production rather than mitochondrial respiration (*Krutzfeldt et al., 1990*), AMIECs display low levels of glycolysis, as attested by low glucose consumption and downregulation of PFKFB3, which catalyzes the production of fructose-2,6-bisP (F2,6BP), a potent allosteric activator of the glycolysis rate-limiting enzyme 6-phosphofructokinase-1 (PFK-1), while also displaying a high membrane potential, suggestive of a high mitochondrial activity. Consistent with high levels of mitochondrial activity, AMIECs displayt a high intracellular content of ROS. The combination of high membrane potential and high ROS levels suggest robust proton coupling at the inner mitochondrial membrane, as uncoupling through the expression of UCP1 or use of pharmacological uncouplers

has been shown to mitigate ROS production (*Cadenas, 2018*). We have found that the augmented ROS content is counteracted in AMIECs by an augmented intracellular content of glutathione, a physiological homeostatic mechanism to prevent damage from excess ROS (*Hayes et al., 2020*). We also provide evidence that the major pathways enabling the biosynthesis of glutathione, the PPP and glutaminolysis, are overactivated in AIMECs as compared to control coronary ECs. The relatively low levels of expression of PFKFB3 and high levels of PFKFB4 point to a shunting of glycolysis towards the PPP in AMIECs, in order to produce NADPH.

Both PFKFB4 and PFKFB3 are upregulated in hypoxia through transcriptional activation by HIF-1α (*Minchenko et al., 2014*), the mTOR pathway (*Feng and Wu, 2017*) and peroxisome proliferator-activating receptor γ (PPARγ) (*Shu et al., 2016*). On the other hand, although wild-type p53, activated in response to DNA damage, transcriptionally represses both PFKFB3 and PFKFB4, PFKFB4, but not PFKFB3, has been described as strongly upregulated in the absence of p53 (*Ros et al., 2017*).

While, similar to HIF-1α, mTOR and PPARγ drive glycolysis, our patient-derived endothelial cells show evidence of diminished glycolysis accompanied with low expression levels of PFKFB3, and thus it seems unlikely that the high levels of PFKFB4 observed in these cells are a downstream outcome of the activation of these pathways. The hypothesis of a blunted function of p53 as a driver of PFKFB4 upregulation in these cells could merit further investigation. Interestingly, the malic enzyme isoforms, ME1 and ME2, are also under negative regulation by p53 and are upregulated in the absence of p53 (*Ros et al., 2017*). Regardless of the mechanisms underlying PFKFB3 low-expression along with PFKFB4 over-expression in AMIECs, predicted downstream consequences are (1) decreased levels of F-2,6-P2 resulting in low PFK1 activity and diminished glycolytic flux, which is consistent with the observed phenotypes, and (2) shunting of G6P towards the pentose phosphate pathway (PPP), reinforced by the activation by PFKFB4 of steroid receptor coactivator-3 (SRC-3), enhancing its transcriptional activity and stimulating the expression of transketolase (TKT) (*Dasgupta et al., 2018*).

The high levels of lactate production observed in AMIECs, concomitant with low glucose consumption, represent a conundrum. High lactate production is frequently linked to strong glycolytic activity, as the glycolytic end-product, pyruvate, can be converted to lactate catalyzed by the enzymatic activity of lactate dehydrogenase-A

(LDH-A). Indeed, in highly proliferating cells, such as cancer or progenitor cells, a high rate of glycolysis can be accompanied with an inhibition of the mitochondrial entry of pyruvate, which, instead, is diverted towards the generation of lactate, a metabolic rewiring designated the Warburg effect, or aerobic glycolysis (*Burns and Manda, 2017*). Strong glycolysis coupled to high lactate production and mitochondrial shutdown is also characteristic of hypoxia, through transcriptional regulation by HIF-1α of key regulators of these three processes, and has been observed in dysfunctional endothelial cells associated with atherosclerosis and vascular diseases (*Fitzgerald et al., 2018; Theodorou and Boon, 2018*).

In the LDH-A catalyzed reaction, pyruvate accepts electrons from NADH, yielding lactate and replenishing NAD^+, predicted to be depleted in AMIECs by a strong drive to produce reducing equivalents and by the increased mitochondrial membrane potential, which impairs electron transport and NAD+ regeneration (*Luengo et al., 2021*). However, under conditions of low glucose consumption and evidence of low glycolytic activity, an alternative source is needed that may explain high lactate production from pyruvate in AMIECs. One possibility is through glutamine-initiated metabolism (*Zielke et al., 1980*), which would be consistent with the strong glutamine consumption observed in AMIECs. In this regard, it has been shown in pancreatic cancer cells that glutamine-derived pyruvate plays a significant role in redox homeostasis.

Collectively, our observations and evidence by others suggest the occurrence of two cell-autonomous, primary deficiencies in AMI patient-derived ECs, namely (1) a strong proton coupling in the mitochondrial membrane that results in excess ROS production, countered by enhanced NADPH and glutathione levels, driven by a glycolysis-to-PPP shunt and an enhanced glutamine metabolism; and (2) a switch in carbon source preference from glucose to glutamine, possibly as an adaptive mechanism aimed at potentiating the production of glutathione, while employing alternative pyruvate-to-lactate conversion pathways that replenish NAD+, thus maintaining a viable redox homeostasis (*Kerk et al., 2022*).

Primary dysfunctions in mitochondria, from either inherited or acquired genetic defects, have been suggested as underlying causes of atherogenic pathologies (*Dabravolski et al., 2022*). Alternatively, our AIMECs might continue to carry, *ex-vivo*, epigenetic imprints of their exposure to factors and cells while in the patients, which

could determine altered phenotypes through many cellular generations. Independent of the original insult, a possible intervention to revert the observed mitochondrial dysfunction would be the use of pharmacological uncouplers to mitigate ROS production and the accompanying metabolic reprogramming (*Cadenas, 2018*). Relevantly, knockout of the uncoupling protein UCP1 caused vascular dysfunction, atherogenesis, and NLRP3 inflammasome activation and IL1-β-dependent inflammation, relieved by re-expression of UCP1 or treatment of animals with chemical uncouplers (*Gu et al., 2021*).

Methods

Endothelial cells

Acute myocardial infection patient-derived endothelial cells (AMIECs) were isolated from coronary atherothrombotic specimens in patients undergoing percutaneous coronary intervention with thrombectomy for the treatment of acute ST-segment elevation myocardial infarction (STEMI) at the Royal Infirmary of Edinburgh, Scotland, UK. Relevant clinical features of the patients are summarized in Table 1. The study protocol was approved by the Institutional Research Ethics Committee, and all subjects provided written informed consent. Specimens were washed with phosphate-buffered saline (PBS) and manually disaggregated. Tissue explants were seeded onto collagen-I coated 6-well plates and maintained under standard cell culture conditions. After 24 hours, tissue explants, non-adherent cells, and debris were aspirated. The medium was changed every other day until the first passage of coronary endothelial outgrowth cells emerged and cells were cultured as described (*Brittan et al., 2015; Padfield et al., 2013; Tura et al., 2013*), on 0.2% gelatin-coated plates with EGM-2 bulletkit medium (Lonza, Basel, Switzerland), containing EBM-2 basal medium along with the EGM-2 singlequots kit components, 10% fetal bovine serum (FBS) and penicillin-streptomycin. Human coronary artery endothelial cells (HCAECs) were purchased from Lonza Clonetics (Walkersville, USA) and used as controls. All cell cultures were maintained in a 37 °C humidified incubator at 5% CO2.

Cell proliferation and viability assays

Cells were counted either with a Scepter Handheld Automated Cell Counter (Merck Millipore, Billerica, MA, USA) or by Hoechst nuclear staining (HO33342, Sigma-Aldrich) (*Aguilar et al., 2016*).

In vitro migration (wound healing) assay

Cells were cultured on 12-well plates in complete medium supplemented with 10% FBS and antibiotics. After reaching confluence, cells starved for one hour in medium containing 0.5% FBS and mitomycin C (1 mg/mL), a cytostatic drug that reacts covalently with DNA forming crosslinks between the complementary strands of DNA, preventing the separation of the complementary DNA strands and inhibiting DNA replication.

Tubulogenesis assay

Endothelial tube formation was monitored using an in vitro angiogenesis assay kit (Merck Millipore ECM625) following the manufacturer's instructions. Briefly, EC cells were cultured in 96 wells plates coated with 5% Matrigel (growth factor-free, Corning # 354230) in EGM2 medium without FBS and supplemented with 1% non-essential amino-acids and antibiotics and left in the incubator for 12 hours. Tube branching points were scored in 5 random fields per concentration using the Angiogenesis plug-in of the Image J software.

Western blotting

70-80% confluent cells were harvested by trypsinization, washed 2x with cold PBS, pellets resuspended in RIPA buffer (50 mM Tris pH 8.0, 150 mM NaCl, 0.1% SDS, 1% Triton X-100 and 0.5% sodium deoxycholate) supplemented with protease inhibitor cocktail (Sigma-Aldrich) and incubated on ice for 5-10 min. Equal amounts of protein per sample were electrophoresed on 8% or 12% SDS-PAGE and subjected to Western blotting.

Quantification of metabolites

Glucose, lactate, glutamate, and glutamine were determined by spectrophotometry (COBAS Mira Plus, Horiba ABX) from cell culture media by monitoring the production of NAD(P)H in specific reactions for each metabolite at 340 nm.

Analysis of polar intracellular metabolites (TCA cycle intermediates and amino acids)

Cells were grown to 70-80% confluence at the required condition for each cellular model and then media removed, and plates washed with ice-cold PBS. TCA cycle intermediates were extracted with addition of 100% methanol:H2O (1:1) mixture and scrapping on ice; then, the extracts were sonicated using a titanium probe (VibraCell, Sonics & Materials Inc., 3 cycles of 5 seconds), chloroform added to the lysates and tubes placed in a shaker for vigorous agitation at 4 °C for 30 min. Subsequently, samples were centrifuged and the upper aqueous phase was separated and evaporated under airflow at room temperature, adding dichloromethane (CH_2Cl_2) for complete dehydration of the samples. TCA cycle intermediates were derivatized by adding 2% (v/v) methoxyamine hidrochloride in pyriridine and shaken vigorously at 37 °C for 90 min. Next, N-methyl-N- (tert-butyldimethylsilyl) trifluoroacetamide (MBTSTFA) and 1% tertbutyldimetheylchlorosilane (TBDMCS) were added, samples incubated for 1 h at 55 °C and finally transferred to GC/MS vials. GC/MS analysis was performed under an electron impact ionization model (*Cascante and Marin, 2008; Dettmer et al., 2007*). The relative concentration of the polar intracellular metabolites is quantified using Norvaline (1mg/mL) as an internal standard.

Glucose-6-phosphate dehydrogenase activity

Cell extracts were prepared using lysis buffer (20 mM Tris-HCl, supplemented with 1 mM DTT, 1 mM EDTA, 0.02% (v/v) Triton X-100, 0.02% (v/v) sodium deoxycholate and protease inhibition cocktail (Sigma-Aldrich). Lysates were sonicated (VibraCell, Sonics & Materials Inc.) and centrifuged at 12,000x g for 20 min at 4 °C. G6PDH specific activity was measured by adding samples to a cuvette containing 0.5 mM $NADP^+$ in 50 mM Tris-HCl, pH 7.6, at 37 °C. The reaction was initiated by the addition of glucose-6-phosphateat at a final concentration of 2 mM (*Aguilar et al., 2016*).

Intracellular ROS determination

Total intracellular ROS levels were determined by means of flow cytometry using the H2DCFDA probe (Invitrogen). Cells were incubated with incubation buffer (5.5 mM glucose in PBS containing 5 µM H_2DCFDA for 30 min at 37 °C and 5% CO_2.

GSH/GSSG quantification

Fresh cells were lysed with 5% 5-sulfosalicylic acid (Sigma-Aldrich) solution, vortexed and disrupted by two freeze/thaw cycles in liquid N_2 and 37 °C water bath. Fifty µL of this solution were separated for subsequent protein quantification. Cell extracts were kept at 4 °C for 10 min and centrifuged at 10,000x g for 10 min. For glutathione quantification, 15 U/mL of glutathione reductase and 40 µg/mL of 5,5'-dithiobis(2-nitrobenzoic acid) (Sigma-Aldrich) were dissolved in assay buffer (100 mM K_2HPO_4/KH_2PO_4, 1 mM EDTA, pH 7.0).

Mitochondrial membrane potential

Cells were incubated with MitoProbe™ DiIC1(5) (1,1′,3,3,3′,3′-hexamethylindodicarbo -cyanine iodide) with or without CCCP (carbonyl cyanide 3-chlorophenylhydrazone) as a mitochondrial membrane potential disruptor, and scored by flow cytometry.

Detailed protocols are available upon request.

Acknowledgments

The project leading to this work has received funding from: The European Commission Horizon 2020 research and innovation program under the MOGLYNET H2020-MSCA-ITN-EJD grant (agreement No 675527); CIBER- Carlos III National Institute of Health, Spain (TT and MC: CIBEREHD-CB17/04/00023; OTC: CIBERES-CP17/00114); Spanish Ministerio de Economia y Competitividad (MINECO) and Ministerio de Ciencia e Innovación -European Commission FEDER funds—"Una manera de hacer Europa" (TT: PID2019-107139RB-C21 and MC: PID2020-115051RB-I00); Generalitat de Catalunya-AGAUR (MC: ICREA Academia Prize 2021, MC: 2021 SGR00350; TT: 2021 SGR1490); Plataforma Temática Interdisciplinar – Salud Global (TT: SGL2103019); NLM is supported by the British Heart Foundation (RE/18/5/34216, RG/20/10/34966, CH/F/21/90010).

References

Aguilar, E, Marin de Mas, I, Zodda, E, Marin, S, Morrish, F, Selivanov, V, Meca-Cortes, O, Delowar, H, Pons, M, Izquierdo, I, Celia-Terrassa, T, de Atauri, P, Centelles, JJ, Hockenbery, D, Thomson, TM, and Cascante, M. 2016. Metabolic Reprogramming and Dependencies Associated with Epithelial Cancer Stem Cells Independent of the Epithelial-Mesenchymal Transition Program. *Stem Cells* **34**: 1163-1176. 10.1002/stem.2286.

Badimon, L, Padro, T, and Vilahur, G. 2012. Atherosclerosis, platelets and thrombosis in acute ischaemic heart disease. *Eur Heart J Acute Cardiovasc Care* **1**: 60-74. 10.1177/2048872612441582.

Benito, A, Polat, IH, Noe, V, Ciudad, CJ, Marin, S, and Cascante, M. 2017. Glucose-6-phosphate dehydrogenase and transketolase modulate breast cancer cell metabolic reprogramming and correlate with poor patient outcome. *Oncotarget* **8**: 106693-106706. 10.18632/oncotarget.21601.

Bensaad, K, Tsuruta, A, Selak, MA, Vidal, MN, Nakano, K, Bartrons, R, Gottlieb, E, and Vousden, KH. 2006. TIGAR, a p53-inducible regulator of glycolysis and apoptosis. *Cell* **126**: 107-120. 10.1016/j.cell.2006.05.036.

Bester, AC, Roniger, M, Oren, YS, Im, MM, Sarni, D, Chaoat, M, Bensimon, A, Zamir, G, Shewach, DS, and Kerem, B. 2011. Nucleotide deficiency promotes genomic instability in early stages of cancer development. *Cell* **145**: 435-446. 10.1016/j.cell.2011.03.044.

Botts, SR, Fish, JE, and Howe, KL. 2021. Dysfunctional Vascular Endothelium as a Driver of Atherosclerosis: Emerging Insights Into Pathogenesis and Treatment. *Front Pharmacol* **12**: 787541. 10.3389/fphar.2021.787541.

Brittan, M, Hunter, A, Boulberdaa, M, Fujisawa, T, Skinner, EM, Shah, AS, Baker, AH, and Mills, NL. 2015. Impaired vascular function and repair in patients with premature coronary artery disease. *Eur J Prev Cardiol* **22**: 1557-1566. 10.1177/2047487315600169.

Brooks, GA. 2018. The Science and Translation of Lactate Shuttle Theory. *Cell Metab* **27**: 757-785. 10.1016/j.cmet.2018.03.008.

Burns, JS, and Manda, G. 2017. Metabolic Pathways of the Warburg Effect in Health and Disease: Perspectives of Choice, Chain or Chance. *Int J Mol Sci* **18**. 10.3390/ijms18122755.

Cadenas, S. 2018. Mitochondrial uncoupling, ROS generation and cardioprotection. *Biochim Biophys Acta Bioenerg* **1859**: 940-950. 10.1016/j.bbabio.2018.05.019.

Cascante, M, and Marin, S. 2008. Metabolomics and fluxomics approaches. *Essays Biochem* **45**: 67-81. 10.1042/BSE0450067.

Dabravolski, SA, Nikiforov, NG, Zhuravlev, AD, Orekhov, NA, Grechko, AV, and Orekhov, AN. 2022. Role of the mtDNA Mutations and Mitophagy in Inflammaging. *Int J Mol Sci* **23**. 10.3390/ijms23031323.

Dasgupta, S, Rajapakshe, K, Zhu, B, Nikolai, BC, Yi, P, Putluri, N, Choi, JM, Jung, SY, Coarfa, C, Westbrook, TF, Zhang, XH, Foulds, CE, Tsai, SY, Tsai, MJ, and O'Malley, BW. 2018. Metabolic enzyme PFKFB4 activates transcriptional coactivator SRC-3 to drive breast cancer. *Nature* **556**: 249-254. 10.1038/s41586-018-0018-1.

De Bock, K, Georgiadou, M, Schoors, S, Kuchnio, A, Wong, BW, Cantelmo, AR, Quaegebeur, A, Ghesquiere, B, Cauwenberghs, S, Eelen, G, Phng, LK, Betz, I, Tembuyser, B, Brepoels, K, Welti, J, Geudens, I, Segura, I, Cruys, B, Bifari, F, Decimo, I, Blanco, R, Wyns, S, Vangindertael, J, Rocha, S, Collins, RT, Munck, S, Daelemans, D, Imamura, H, Devlieger, R, Rider, M, Van Veldhoven, PP, Schuit, F, Bartrons, R, Hofkens, J, Fraisl, P, Telang, S, Deberardinis, RJ, Schoonjans, L, Vinckier, S, Chesney, J, Gerhardt, H, Dewerchin, M, and Carmeliet, P. 2013. Role of PFKFB3-driven glycolysis in vessel sprouting. *Cell* **154**: 651-663. 10.1016/j.cell.2013.06.037.

DeBerardinis, RJ, and Cheng, T. 2010. Q's next: the diverse functions of glutamine in metabolism, cell biology and cancer. *Oncogene* **29**: 313-324. 10.1038/onc.2009.358.

Dettmer, K, Aronov, PA, and Hammock, BD. 2007. Mass spectrometry-based metabolomics. *Mass Spectrom Rev* **26**: 51-78. 10.1002/mas.20108.

Draoui, N, de Zeeuw, P, and Carmeliet, P. 2017. Angiogenesis revisited from a metabolic perspective: role and therapeutic implications of endothelial cell metabolism. *Open Biol* **7**. 10.1098/rsob.170219.

Dromparis, P, and Michelakis, ED. 2013. Mitochondria in vascular health and disease. *Annu Rev Physiol* **75**: 95-126. 10.1146/annurev-physiol-030212-183804.

Eelen, G, de Zeeuw, P, Treps, L, Harjes, U, Wong, BW, and Carmeliet, P. 2018. Endothelial Cell Metabolism. *Physiol Rev* **98**: 3-58. 10.1152/physrev.00001.2017.

Feng, Y, and Wu, L. 2017. mTOR up-regulation of PFKFB3 is essential for acute myeloid leukemia cell survival. *Biochem Biophys Res Commun* **483**: 897-903. 10.1016/j.bbrc.2017.01.031.

Fitzgerald, G, Soro-Arnaiz, I, and De Bock, K. 2018. The Warburg Effect in Endothelial Cells and its Potential as an Anti-angiogenic Target in Cancer. *Front Cell Dev Biol* **6**: 100. 10.3389/fcell.2018.00100.

Gallogly, S, Fujisawa, T, Hung, JD, Brittan, M, Skinner, EM, Mitchell, AJ, Medine, C, Luque, N, Zodda, E, Cascante, M, Hadoke, PW, Mills, NL, and Tura-Ceide, O. 2021. Generation of a Novel In Vitro Model to Study Endothelial Dysfunction from Atherothrombotic Specimens. *Cardiovasc Drugs Ther* **35**: 1281-1290. 10.1007/s10557-021-07151-9.

Goveia, J, Stapor, P, and Carmeliet, P. 2014. Principles of targeting endothelial cell metabolism to treat angiogenesis and endothelial cell dysfunction in disease. *EMBO Mol Med* **6**: 1105-1120. 10.15252/emmm.201404156.

Grajeda-Iglesias, C, and Aviram, M. 2018. Specific Amino Acids Affect Cardiovascular Diseases and Atherogenesis via Protection against Macrophage Foam Cell Formation: Review Article. *Rambam Maimonides Med J* **9**. 10.5041/RMMJ.10337.

Gu, P, Hui, X, Zheng, Q, Gao, Y, Jin, L, Jiang, W, Zhou, C, Liu, T, Huang, Y, Liu, Q, Nie, T, Wang, Y, Wang, Y, Zhao, J, and Xu, A. 2021. Mitochondrial uncoupling protein 1 antagonizes atherosclerosis by blocking NLRP3 inflammasome-dependent interleukin-1beta production. *Sci Adv* **7**: eabl4024. 10.1126/sciadv.abl4024.

Hayes, JD, Dinkova-Kostova, AT, and Tew, KD. 2020. Oxidative Stress in Cancer. *Cancer Cell* **38**: 167-197. 10.1016/j.ccell.2020.06.001.

Ishimoto, T, Nagano, O, Yae, T, Tamada, M, Motohara, T, Oshima, H, Oshima, M, Ikeda, T, Asaba, R, Yagi, H, Masuko, T, Shimizu, T, Ishikawa, T, Kai, K, Takahashi, E, Imamura, Y, Baba, Y, Ohmura, M, Suematsu, M, Baba, H, and Saya, H. 2011. CD44 variant regulates redox status in cancer cells by stabilizing the xCT subunit of system xc(-) and thereby promotes tumor growth. *Cancer Cell* **19**: 387-400. 10.1016/j.ccr.2011.01.038.

Kerk, SA, Lin, L, Myers, AL, Sutton, DJ, Andren, A, Sajjakulnukit, P, Zhang, L, Zhang, Y, Jimenez, JA, Nelson, BS, Chen, B, Robinson, A, Thurston, G, Kemp, SB, Steele, NG, Hoffman, MT, Wen, HJ, Long, D, Ackenhusen, SE, Ramos, J, Gao, X, Nwosu, ZC, Galban, S, Halbrook, CJ, Lombard, DB, Piwnica-Worms, DR, Ying, H, Pasca di Magliano, M, Crawford, HC, Shah, YM, and Lyssiotis, CA. 2022. Metabolic requirement for GOT2 in pancreatic cancer depends on environmental context. *Elife* **11**. 10.7554/eLife.73245.

Krutzfeldt, A, Spahr, R, Mertens, S, Siegmund, B, and Piper, HM. 1990. Metabolism of exogenous substrates by coronary endothelial cells in culture. *J Mol Cell Cardiol* **22**: 1393-1404. 10.1016/0022-2828(90)90984-a.

Laplante, M, and Sabatini, DM. 2012. mTOR signaling in growth control and disease. *Cell* **149**: 274-293. 10.1016/j.cell.2012.03.017.

Li, H, Horke, S, and Forstermann, U. 2014. Vascular oxidative stress, nitric oxide and atherosclerosis. *Atherosclerosis* **237**: 208-219. 10.1016/j.atherosclerosis.2014.09.001.

Li, X, Kumar, A, and Carmeliet, P. 2019. Metabolic Pathways Fueling the Endothelial Cell Drive. *Annu Rev Physiol* **81**: 483-503. 10.1146/annurev-physiol-020518-114731.

Luengo, A, Li, Z, Gui, DY, Sullivan, LB, Zagorulya, M, Do, BT, Ferreira, R, Naamati, A, Ali, A, Lewis, CA, Thomas, CJ, Spranger, S, Matheson, NJ, and Vander Heiden, MG. 2021. Increased demand for NAD(+) relative to ATP drives aerobic glycolysis. *Mol Cell* **81**: 691-707 e696. 10.1016/j.molcel.2020.12.012.

Minchenko, OH, Tsuchihara, K, Minchenko, DO, Bikfalvi, A, and Esumi, H. 2014. Mechanisms of regulation of PFKFB expression in pancreatic and gastric cancer cells. *World J Gastroenterol* **20**: 13705-13717. 10.3748/wjg.v20.i38.13705.

Moreno-Viedma, V, Amor, M, Sarabi, A, Bilban, M, Staffler, G, Zeyda, M, and Stulnig, TM. 2016. Common dysregulated pathways in obese adipose tissue and atherosclerosis. *Cardiovasc Diabetol* **15**: 120. 10.1186/s12933-016-0441-2.

Murphy, MP. 2009. How mitochondria produce reactive oxygen species. *Biochem J* **417**: 1-13. 10.1042/BJ20081386.

Negre-Salvayre, A, Guerby, P, Gayral, S, Laffargue, M, and Salvayre, R. 2020. Role of reactive oxygen species in atherosclerosis: Lessons from murine genetic models. *Free Radic Biol Med* **149**: 8-22. 10.1016/j.freeradbiomed.2019.10.011.

Padfield, GJ, Tura-Ceide, O, Freyer, E, Barclay, GR, Turner, M, Newby, DE, and Mills, NL. 2013. Endothelial progenitor cells, atheroma burden and clinical outcome in patients with coronary artery disease. *Heart* **99**: 791-798. 10.1136/heartjnl-2012-302949.

Previtali, E, Bucciarelli, P, Passamonti, SM, and Martinelli, I. 2011. Risk factors for venous and arterial thrombosis. *Blood Transfus* **9**: 120-138. 10.2450/2010.0066-10.

Ros, S, Floter, J, Kaymak, I, Da Costa, C, Houddane, A, Dubuis, S, Griffiths, B, Mitter, R, Walz, S, Blake, S, Behrens, A, Brindle, KM, Zamboni, N, Rider, MH, and Schulze, A. 2017. 6-Phosphofructo-2-kinase/fructose-2,6-biphosphatase 4 is essential for p53-null cancer cells. *Oncogene* **36**: 3287-3299. 10.1038/onc.2016.477.

Schoors, S, De Bock, K, Cantelmo, AR, Georgiadou, M, Ghesquiere, B, Cauwenberghs, S, Kuchnio, A, Wong, BW, Quaegebeur, A, Goveia, J, Bifari, F, Wang, X, Blanco, R, Tembuyser, B, Cornelissen, I, Bouche, A, Vinckier, S, Diaz-Moralli, S, Gerhardt, H, Telang, S, Cascante, M, Chesney, J, Dewerchin, M, and Carmeliet, P. 2014. Partial and transient reduction of glycolysis by PFKFB3 blockade reduces pathological angiogenesis. *Cell Metab* **19**: 37-48. 10.1016/j.cmet.2013.11.008.

Seo, M, and Lee, YH. 2014. PFKFB3 regulates oxidative stress homeostasis via its S-glutathionylation in cancer. *J Mol Biol* **426**: 830-842. 10.1016/j.jmb.2013.11.021.

Shemiakova, T, Ivanova, E, Grechko, AV, Gerasimova, EV, Sobenin, IA, and Orekhov, AN. 2020. Mitochondrial Dysfunction and DNA Damage in the Context of Pathogenesis of Atherosclerosis. *Biomedicines* **8**. 10.3390/biomedicines8060166.

Shu, Y, Lu, Y, Pang, X, Zheng, W, Huang, Y, Li, J, Ji, J, Zhang, C, and Shen, P. 2016. Phosphorylation of PPARgamma at Ser84 promotes glycolysis and cell proliferation in hepatocellular carcinoma by targeting PFKFB4. *Oncotarget* **7**: 76984-76994. 10.18632/oncotarget.12764.

Smolders, VF, Zodda, E, Quax, PHA, Carini, M, Barbera, JA, Thomson, TM, Tura-Ceide, O, and Cascante, M. 2018. Metabolic Alterations in Cardiopulmonary Vascular Dysfunction. *Front Mol Biosci* **5**: 120. 10.3389/fmolb.2018.00120.

Sun, L, Kong, Y, Cao, M, Zhou, H, Li, H, Cui, Y, Fang, F, Zhang, W, Li, J, Zhu, X, Li, Q, Song, T, and Zhang, T. 2017. Decreased expression of acetyl-CoA synthase 2 promotes metastasis and predicts poor prognosis in hepatocellular carcinoma. *Cancer Sci* **108**: 1338-1346. 10.1111/cas.13252.

Thangavelu, K, Chong, QY, Low, BC, and Sivaraman, J. 2014. Structural basis for the active site inhibition mechanism of human kidney-type glutaminase (KGA). *Sci Rep* **4**: 3827. 10.1038/srep03827.

Theodorou, K, and Boon, RA. 2018. Endothelial Cell Metabolism in Atherosclerosis. *Front Cell Dev Biol* **6**: 82. 10.3389/fcell.2018.00082.

Townsend, N, Kazakiewicz, D, Lucy Wright, F, Timmis, A, Huculeci, R, Torbica, A, Gale, CP, Achenbach, S, Weidinger, F, and Vardas, P. 2022. Epidemiology of cardiovascular disease in Europe. *Nat Rev Cardiol* **19**: 133-143. 10.1038/s41569-021-00607-3.

Tura, O, Skinner, EM, Barclay, GR, Samuel, K, Gallagher, RC, Brittan, M, Hadoke, PW, Newby, DE, Turner, ML, and Mills, NL. 2013. Late outgrowth endothelial cells resemble mature endothelial cells and are not derived from bone marrow. *Stem Cells* **31**: 338-348. 10.1002/stem.1280.

van den Heuvel, AP, Jing, J, Wooster, RF, and Bachman, KE. 2012. Analysis of glutamine dependency in non-small cell lung cancer: GLS1 splice variant GAC is essential for cancer cell growth. *Cancer Biol Ther* **13**: 1185-1194. 10.4161/cbt.21348.

Wong, CC, Qian, Y, Li, X, Xu, J, Kang, W, Tong, JH, To, KF, Jin, Y, Li, W, Chen, H, Go, MY, Wu, JL, Cheng, KW, Ng, SS, Sung, JJ, Cai, Z, and Yu, J. 2016. SLC25A22 Promotes Proliferation and Survival of Colorectal Cancer Cells With KRAS Mutations and Xenograft Tumor Progression in Mice via Intracellular Synthesis of Aspartate. *Gastroenterology* **151**: 945-960 e946. 10.1053/j.gastro.2016.07.011.

Wurtz, P, Raiko, JR, Magnussen, CG, Soininen, P, Kangas, AJ, Tynkkynen, T, Thomson, R, Laatikainen, R, Savolainen, MJ, Laurikka, J, Kuukasjarvi, P, Tarkka, M, Karhunen, PJ, Jula, A, Viikari, JS, Kahonen, M, Lehtimaki, T, Juonala, M, Ala-Korpela, M, and Raitakari, OT. 2012. High-throughput quantification of circulating metabolites improves prediction of subclinical atherosclerosis. *Eur Heart J* **33**: 2307-2316. 10.1093/eurheartj/ehs020.

Xia, N, Daiber, A, Forstermann, U, and Li, H. 2017. Antioxidant effects of resveratrol in the cardiovascular system. *Br J Pharmacol* **174**: 1633-1646. 10.1111/bph.13492.

Zielke, HR, Sumbilla, CM, Sevdalian, DA, Hawkins, RL, and Ozand, PT. 1980. Lactate: a major product of glutamine metabolism by human diploid fibroblasts. *J Cell Physiol* **104**: 433-441. 10.1002/jcp.1041040316.

802 Zorova, LD, Popkov, VA, Plotnikov, EY, Silachev, DN, Pevzner, IB, Jankauskas, SS,
803 Babenko, VA, Zorov, SD, Balakireva, AV, Juhaszova, M, Sollott, SJ, and Zorov, DB.
804 2018. Mitochondrial membrane potential. *Anal Biochem* **552**: 50-59.
805 10.1016/j.ab.2017.07.009.
806
807
808

	n=8
Age, years	60 ± 15
Gender, male	5 (66%)
Medical history and risk factors	
Previous myocardial infarction	1 (12%)
Previous PCI/CABG	1 (12 %)
Current smoker	3 (37%)
Ex-smoker	2 (25%)
Hypertension	1 (12%)
Hyperlipidaemia	4 (50%)
Family history of premature coronary heart disease	1 (12%)
Diabetes mellitus	0
Medication on admission	
Aspirin	2 (25%)
Clopidogrel	1 (12%)
B-Blockers	1 (12%)
ACE-Inhibitors	1 (12%)
Statins	3 (38%)
Myocardial injury	
Troponin I concentration, micrograms/L	27.9 ± 20.0
Culprit vessel	
Left anterior descending artery, n=12	1
Circumflex artery, n=2	1
Right coronary artery, n=23	4

Table 1: Clinical characteristics of patients providing coronary endothelial outgrowth following thrombectomy for ST-segment elevation myocardial infarction. Values are number (%) or mean ± standard deviation. ACE = angiotensin-converting enzyme; CABG = coronary artery bypass grafting; PCI = percutaneous coronary intervention.

Figure Legends

Figure 1. **AMIECs display impaired growth and migration**. (**A**) Bright field images of HCAECs (left panels) vs. AMIECs (right panels), captured under 10x and 20x objectives on a Leica microscope. (**B**) Representative Western blotting experiments for the endothelial markers, PECAM-1, V-CAM1, CD-34 and CD-10 (Figure 1 source data 1-4). (**C**) Growth rate of AMIECs and control HCAEC, expressed as fold change relative to initial cell number seeded. Error bars represent mean ± SD (n=3). (**D**) Cell cycle analysis of AMIECs and HCAECs under logarithmic growth conditions, showing a non-significant trend for AMIECs to accumulate G1 phase as compared to HCAEC. Error bars represent mean ± SD (n=3). (**E**) Representative images of Mito C-treated migration in scratch wound assays, showing reduced migration of AMIECs compared to control HCAECs. (**F**) Quantification of cell migration in scratch wound assays, represented as % of wound closure. Values are mean ± SD (n = 3). Student's t-test significance values were calculated for AMIECs vs. HCAEC: *p ≤ 0.05 **p ≤ 0.01, ***p ≤ 0.001.

Figure 2. **Defective tubulogenesis of AMIECs**. (**A**) Endothelial tube network formation after 12 h of VEGF stimulation. Shown are representative bright field images from triplicate experiments. Scale bar = 100 μm. (**B**) Tube branch point quantification of images from experiments performed as in (A). Values are mean ± SD (n = 3). Student's t-test significance values were calculated for AMIECs vs. HCAEC: *p ≤ 0.05 **p ≤ 0.01, ***p ≤ 0.001. (**C**) Correlation between relative migration (Fig. 1F) and tubulogenesis in AMIECs and HCAECs.

Figure 3. **AMIECs display low glucose consumption and high lactate production**. (**A**) Glucose consumption and Lactate production have been measured after 48 h. (**B**) Conversion rate of glucose to lactate. Error bars represent mean ± SD (n=3). Student's t-test significance values were calculated for AMIECs vs. HCAECs: *p ≤ 0.05 **p ≤ 0.01 and ***p ≤ 0.001.

Figure 4. **AMIECs shunt glycolysis towards PPP and NADPH generation**. (**A**) Representative Western blotting of PFKFB3 and PFKFB4 in AMIECs and HCAECs (Figure 4 source data 1-2). (**B**) Quantification of band intensities for PFKFB3 and PFKFB4 in triplicate Western blotting experiments, normalized to β-actin band

intensities. Values are mean ± SD (n = 3). (**C**) Representative Western blotting for G6PD in AMIECs and HCAECs (Figure 4 source data 3). (**D**) Quantification of band intensities for G6PD in triplicate Western blotting experiments, normalized to β-actin band intensities. (**E**) G6PD enzyme activities normalized to intracellular protein content (n = 3). (**F**) ROS levels determined by flow cytometry. Results are expressed as the mean fluorescent intensity. (**G**) Total intracellular reduced glutathione content. Values are normalized to cellular protein concentration. Error bars represent mean ± SD (n=3). For all experiments, Student's t-test significance values were calculated for AMIECs vs. HCAECs: *p ≤ 0.05 **p ≤ 0.01 and ***p ≤ 0.001.

Figure 5. **AMIECs display a strong glutamine metabolism**. (**A**) Glutamine and glucose production levels in cell culture medium after 48 h. Negative values reflect net consumption. (**B**) Representative Western blotting experiments in AMIECs and HCAECs for the two major isoforms of GLS1, KGA and GAC, using isoform-specific antibodies (Figure 5 source data 1). (**C**) Quantification of band intensities for KGA and GAC in triplicate Western blotting experiments, normalized to β-actin band intensities. (**D**) Ratio of KGA vs GAC isoform expression levels, calculated from the actin-normalized band intensities quantitated in (C). (**E**) Intracellular amino acid levels (**F**) Glutamate and glutamine production levels in cell culture medium after 48 h. Negative values reflect net consumption. (**G**) Glutamine/glutamate consumption ratio. (**H**) Mitochondrial metabolic potential of AMIECs and control HCAEC cells. Cells were stained with 50 nM $DiIC_1(5)$ without or with of 50 µM carbonyl cyanide 3-chlorophenylhydrazone (CCCP). Error bars represent mean ± SD (n=3). For all experiments, Student's t-test significance values were calculated for AMIECs vs. HCAECs: *p ≤ 0.05 **p ≤ 0.01 and ***p ≤ 0.001.

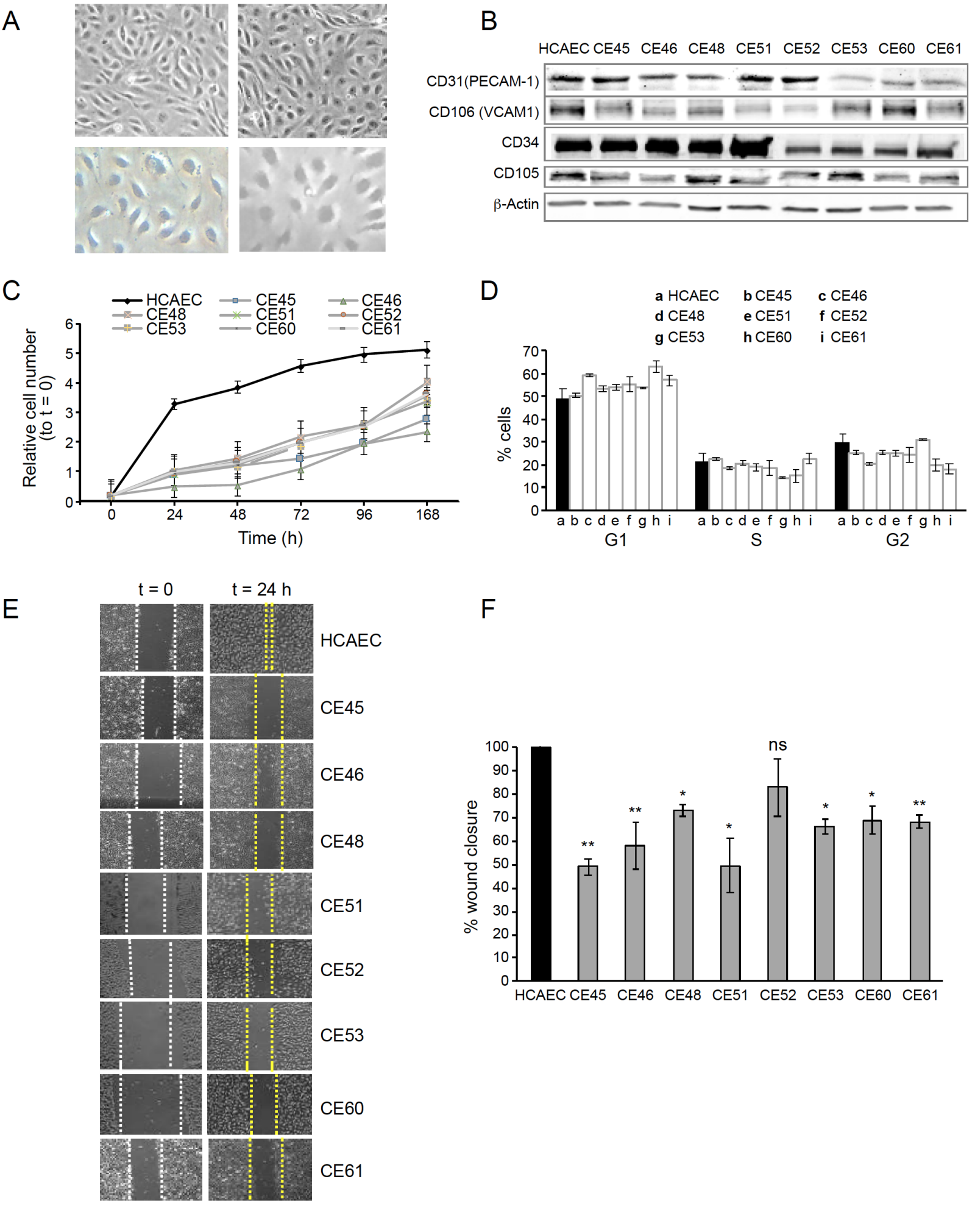
A
B
HCAEC CE45 CE46 CE48 CE51 CE52 CE53 CE60 CE61
CD31(PECAM-1)
CD106 (VCAM1)
CD34
CD105
β-Actin
C
HCAEC
CE45
CE46
CE48
CE51
CE52
CE53
CE60
CE61
Relative cell number (to t = 0)
Time (h)
D
a HCAEC
b CE45
c CE46
d CE48
e CE51
f CE52
g CE53
h CE60
i CE61
% cells
G1
S
G2
E
t = 0
t = 24 h
HCAEC
CE45
CE46
CE48
CE51
CE52
CE53
CE60
CE61
F
% wound closure
ns
HCAEC CE45 CE46 CE48 CE51 CE52 CE53 CE60 CE61

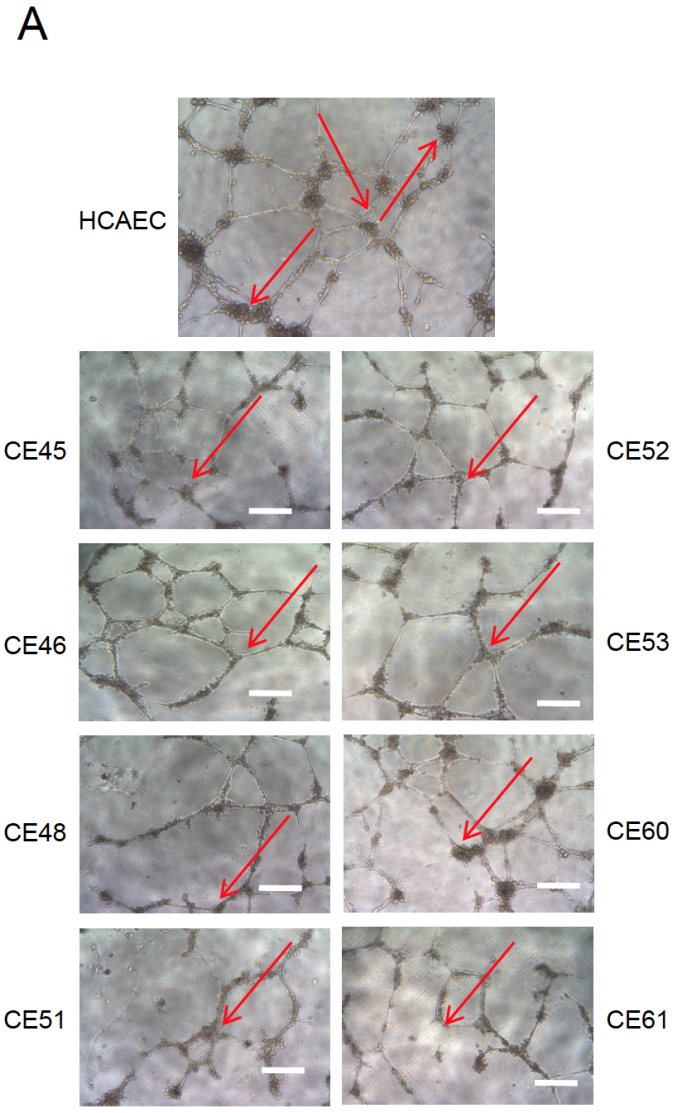
A
HCAEC
CE45
CE52
CE46
CE53
CE48
CE60
CE51
CE61

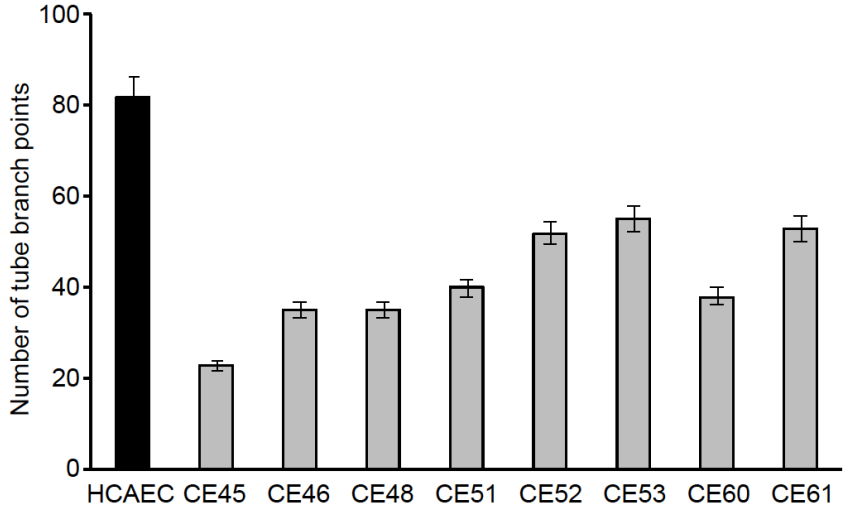
B
Number of tube branch points
100
80
60
40
20
0
HCAEC
CE45
CE46
CE48
CE51
CE52
CE53
CE60
CE61

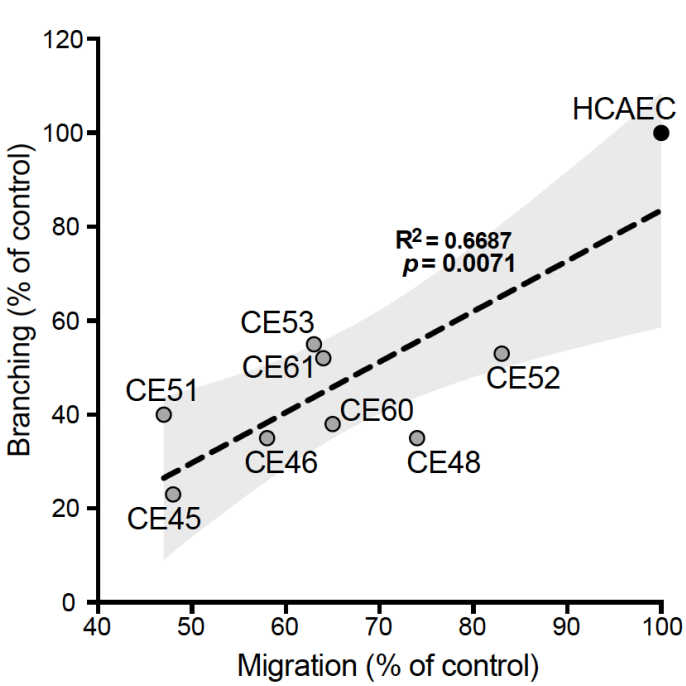
C
Branching (% of control)
Migration (% of control)
120
100
80
60
40
20
0
40
50
60
70
80
90
100
HCAEC
CE53
CE61
CE52
CE51
CE60
CE46
CE48
CE45
R2 = 0.6687
p = 0.0071

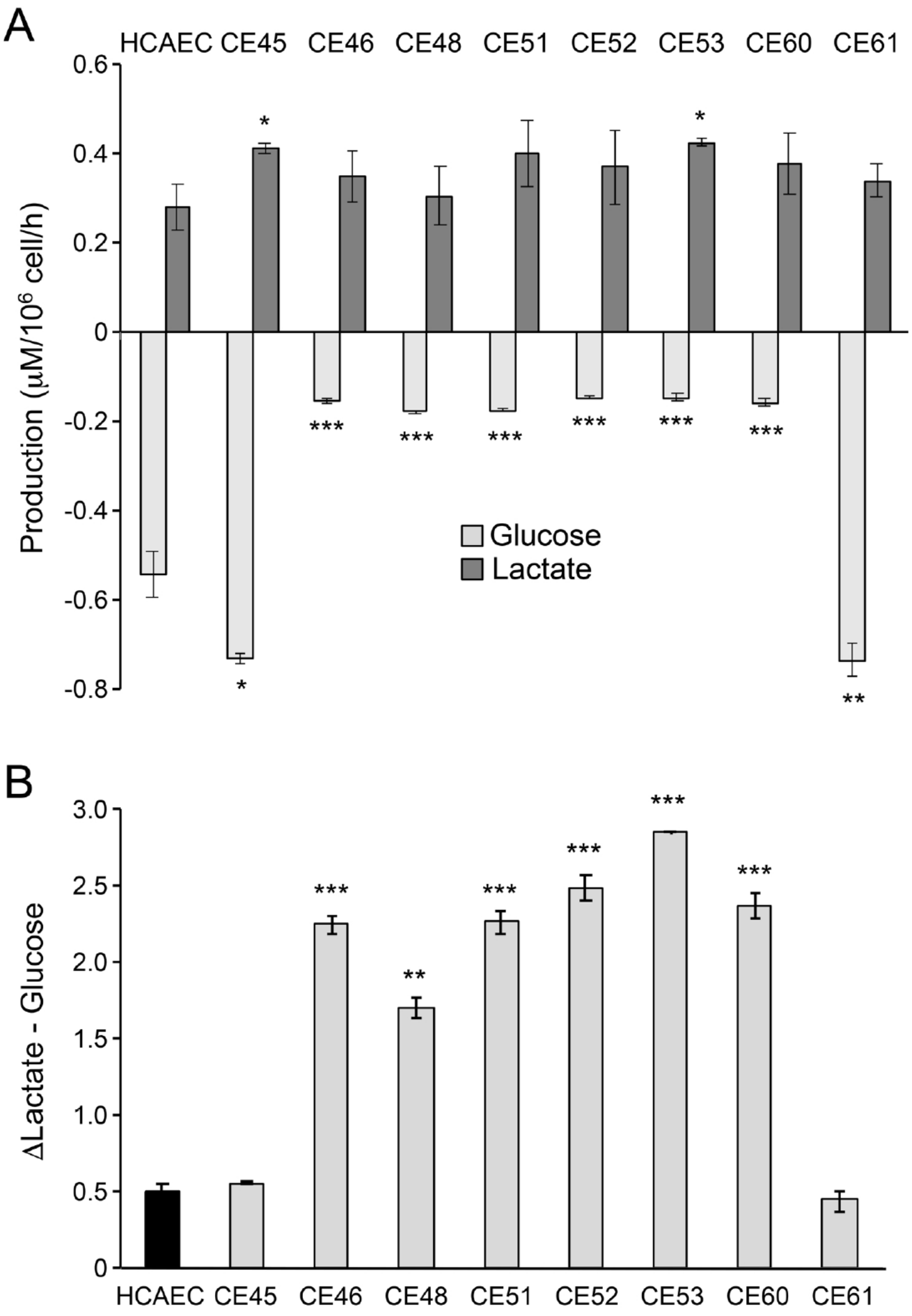
A
HCAEC
CE45
CE46
CE48
CE51
CE52
CE53
CE60
CE61
Production (μM/10^6 cell/h)
0.6
0.4
0.2
0
-0.2
-0.4
-0.6
-0.8
Glucose
Lactate
B
ΔLactate - Glucose
3.0
2.5
2.0
1.5
1.0
0.5
0

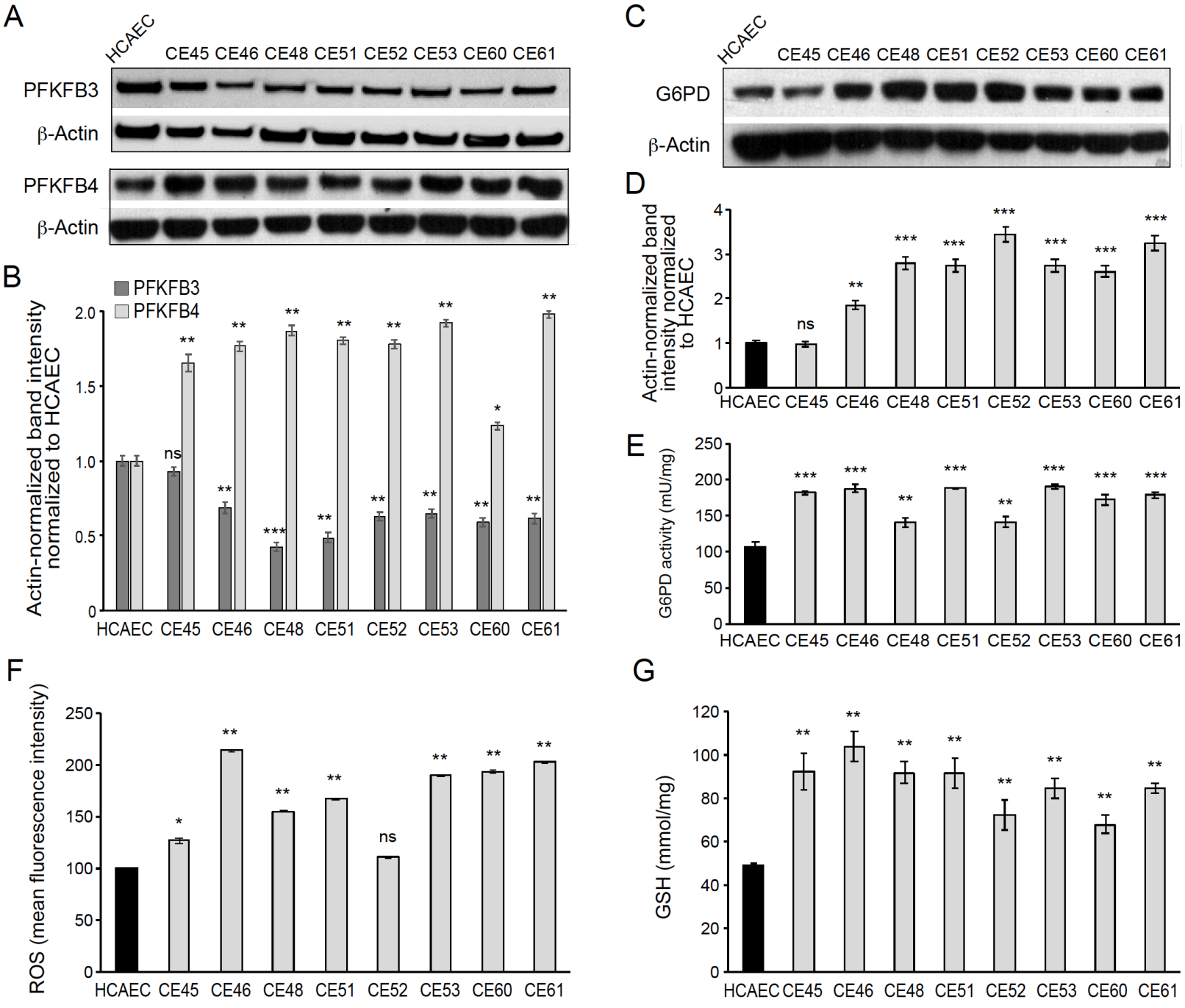
A
HCAEC
CE45 CE46 CE48 CE51 CE52 CE53 CE60 CE61
PFKFB3
β-Actin
PFKFB4
β-Actin
B
PFKFB3
PFKFB4
Actin-normalized band intensity normalized to HCAEC
HCAEC CE45 CE46 CE48 CE51 CE52 CE53 CE60 CE61
C
HCAEC
CE45 CE46 CE48 CE51 CE52 CE53 CE60 CE61
G6PD
β-Actin
D
Actin-normalized band intensity normalized to HCAEC
HCAEC CE45 CE46 CE48 CE51 CE52 CE53 CE60 CE61
E
G6PD activity (mU/mg)
HCAEC CE45 CE46 CE48 CE51 CE52 CE53 CE60 CE61
F
ROS (mean fluorescence intensity)
HCAEC CE45 CE46 CE48 CE51 CE52 CE53 CE60 CE61
G
GSH (mmol/mg)
HCAEC CE45 CE46 CE48 CE51 CE52 CE53 CE60 CE61

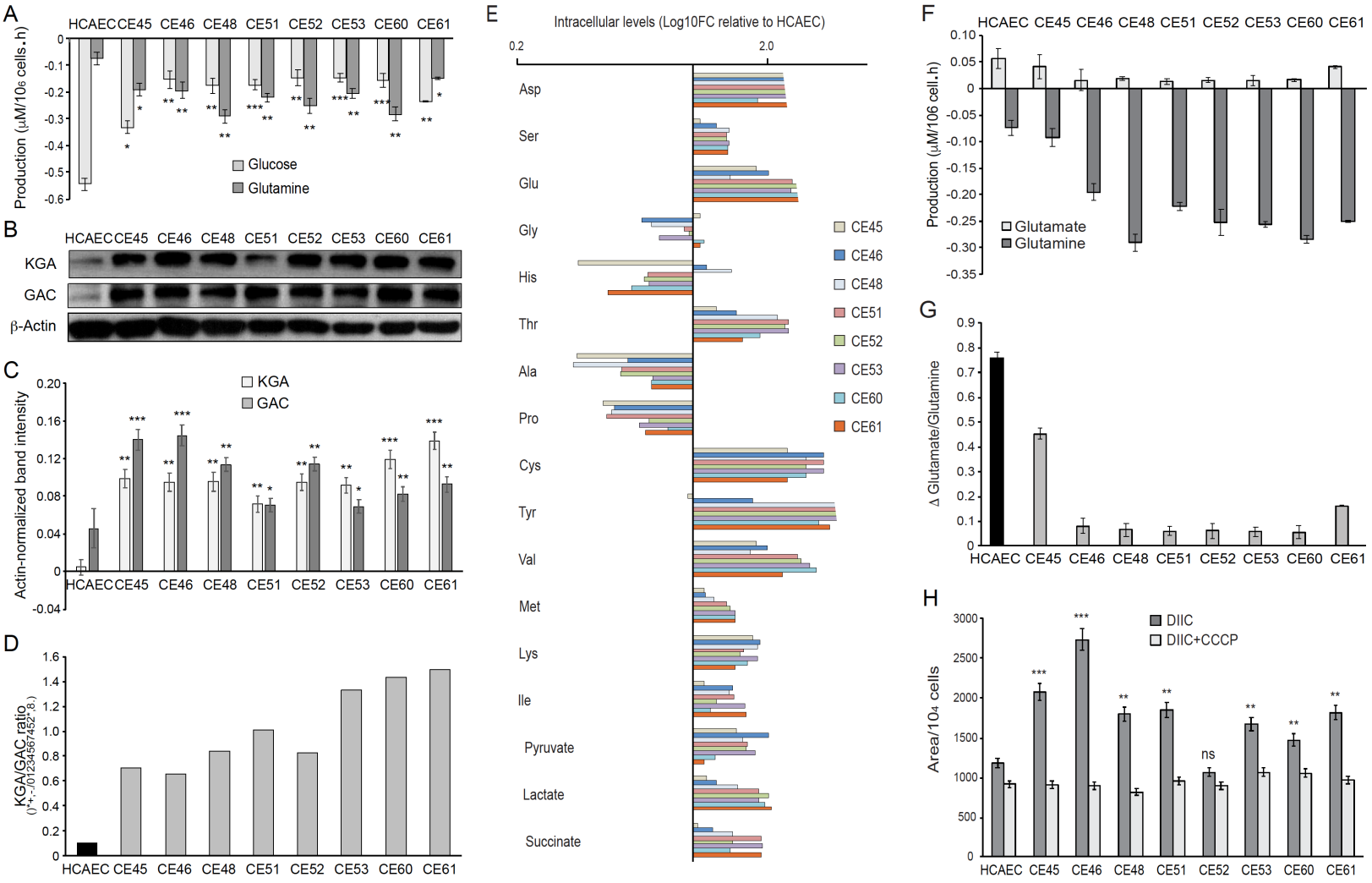
A
HCAEC CE45 CE46 CE48 CE51 CE52 CE53 CE60 CE61
Production (μM/10⁶ cells.h)
Glucose
Glutamine
B
HCAEC CE45 CE46 CE48 CE51 CE52 CE53 CE60 CE61
KGA
GAC
β-Actin
C
KGA
GAC
Actin-normalized band intensity
HCAEC CE45 CE46 CE48 CE51 CE52 CE53 CE60 CE61
D
KGA/GAC ratio
HCAEC CE45 CE46 CE48 CE51 CE52 CE53 CE60 CE61
E
Intracellular levels (Log10FC relative to HCAEC)
0.2
2.0
Asp
Ser
Glu
Gly
His
Thr
Ala
Pro
Cys
Tyr
Val
Met
Lys
Ile
Pyruvate
Lactate
Succinate
CE45
CE46
CE48
CE51
CE52
CE53
CE60
CE61
F
HCAEC CE45 CE46 CE48 CE51 CE52 CE53 CE60 CE61
Production (μM/106 cell.h)
Glutamate
Glutamine
G
Δ Glutamate/Glutamine
HCAEC CE45 CE46 CE48 CE51 CE52 CE53 CE60 CE61
H
Area/10⁴ cells
DIIC
DIIC+CCCP
ns
HCAEC CE45 CE46 CE48 CE51 CE52 CE53 CE60 CE61